PHYSICAL REVIEW A **69**, 013601 (2004)

Quantum superchemistry: Role of trapping profile and quantum statistics

M. K. Olsen
Instituto de Física da Universidade Federal Fluminense, Boa Viagem 24210-340, Niterói, Rio de Janeiro, Brazil
(Received 11 September 2003; published 5 January 2004)

The process of Raman photoassociation of a trapped atomic condensate to form condensed molecules has been labeled superchemistry because it can occur at 0 K and experiences coherent bosonic stimulation. We show here that the differences from ordinary chemical processes go even deeper, with the conversion rates depending on the quantum state of the reactants, as expressed by the Wigner function. We consider different initial quantum states of the trapped atomic condensate and different forms of the confining potentials, demonstrating the importance of the quantum statistics and the extra degrees of freedom which massive particles and trapping potentials make available over the analogous optical process of second-harmonic generation. We show that both mean-field analyses and quantum calculations using an inappropriate initial condition can make inaccurate predictions for a given system. This is possible whether using a spatially dependent analysis or a zero-dimensional approach as commonly used in quantum optics.

DOI: 10.1103/PhysRevA.69.013601 PACS number(s): 03.75.Kk, 03.75.Mn, 05.30.Jp

I. INTRODUCTION

The production of a molecular Bose-Einstein condensate (BEC) via Raman photoassociation of an atomic condensate has attracted a great deal of theoretical and experimental interest in the last few years. That an atom-optical analog of the optical processes of upconversion and down-conversion should exist with atomic and molecular condensates was first stated by Drummond *et al.* [1], who developed an effective quantum field theory to describe coupled atomic and molecular BECs. An early suggestion that a molecular condensate could be produced via photoassociation came from Javanainen and Mackie [2], who proposed a two-mode, phenomenological Hamiltonian to model the process. A more complete proposal, using an atomic and two molecular fields with spatial dependence, coupled via a two-color Raman transition so as to minimize spontaneous emission losses, was developed by Heinzen *et al.* [3], who called this process superchemistry. Their model, using a mean-field, Gross-Pitaevskii equation (GPE) approach, showed that the dynamics were quite different from those of normal chemical reactions. As shown by Hope and Olsen in one dimension [4], and Hope in three dimensions [5], full quantum treatments using the positive-P representation [6,7] and initial coherent states may not always agree with mean-field predictions, as the quantum noise affects the dynamics. In a recent work, Olsen and Plimak [8] showed that the initial quantum state of the atomic condensate, as expressed by the Wigner function, can also have an effect on the dynamics. The present work is an extension of Ref. [8] to consider longer interaction times, different trapping potentials and the efficacy of a single-mode-type approach. A fuller derivation of the equations of motion is also included. Overall, what we will demonstrate is that the superchemistry described in Ref. [3] is even more different from standard chemistry than the original authors supposed. To our knowledge, no chemical process which would depend on the pseudoprobability function of the reactants has been described previously.

Another question which has attracted the attention of theorists has been the issue of the quantum state of a trapped condensate with repulsive interatomic interactions. As far as we are aware, experimentalists have not paid much attention to this issue, despite suggestions for the reconstruction of the density matrix experimentally [9,10]. Perhaps the two most common choices are the well-known coherent state and the number, or Fock state, both much used in quantum optics. The coherent state appeals because of the coherence properties exhibited in interference experiments [11–13], but has the problem of a largish uncertainty in number, which is conceptually difficult to understand as atoms are not created or destroyed at typical temperatures. The number state is superficially an appealing choice, but as the condensate is in contact with an environment, some particles can be added or removed. This state also has the problem that it has no defined phase. Another problem, perhaps more philosophical, is whether we can actually talk about number states when we do not know exactly what the number involved may be. In an actual BEC, the nonlinearity due to s-wave collisions between condensed atoms is equivalent to a Kerr interaction, so that we may expect to find that the actual state is none of the above. Calculations using various approximations have predicted an amplitude eigenstate [14], a sheared Wigner function which approximates a number squeezed state [15], and a Q function which suggests both amplitude quadrature and number squeezing [16]. Another recent work has proposed that generalized coherent states may be a more appropriate description [17].

In this work we combine these two issues, considering the effects of different possible initial states on the dynamics of Raman photoassociation, without actually solving the problem of which may be the most likely ground state of the trapped condensate. As the mathematics of photoassociation is essentially a more complex form of that of second-harmonic generation, and both quantum statistics [18,19] and Kerr nonlinearities [20] have been shown to affect the dynamics of this process, it is of interest to investigate their effect in the present situation. As we are interested only in the dynamics of the mean fields rather than quantum correlations, we stochastically integrate the appropriate equations in the truncated Wigner representation [7,21,22], which we

expect to give reliable results. In fact, as the numbers of interacting particles involved become greater, we can expect that the accuracy will increase. We will also investigate the appropriateness of a zero-dimensional approach to this problem, which necessarily neglects the trapping potential and the kinetic energy of the condensed particles. As there is some experimental freedom in engineering trapping potentials [23], we will also investigate the effect of profiles other than the harmonic one generally used in theoretical analyses.

II. THEORETICAL TREATMENTS OF INTERACTING CONDENSATES

In principle there exist several ways to theoretically model the dynamics of interacting condensates, but in practice we find that our options are somewhat limited. A full and exact treatment requires a description in terms of quantum fields, but as the resulting functional Heisenberg equations of motion are highly nonlinear, this approach is impracticable. An equivalent option, the quantum master equation, is totally impractical as the dimension of the required Hilbert space is far beyond the capacities of any computer. Assuming nonvanishing expectation values for the field operators in the Heisenberg equations leads to the mean-field approach of the GPE [24,25], which, even though it is derived using quantum statistical considerations, cannot describe the effect of these on the dynamics. Worse, for systems of interacting fields, the GPE has been shown to give misleading predictions in some parameter regimes [4,5]. An alternative approach which can say something about the quantum features is path-integral Monte Carlo [26], but this method is only really practical for calculating ground-state properties and not dynamical evolution. Other recent developments have been the use of stochastic wave functions [27] to solve *N*-boson time-dependent problems and a stochastic GPE, developed from the quantum kinetic master equation [28].

The phase-space methods so commonly used in quantum optics have also been extended in a functional form to treat dynamical problems in condensates. These methods provide a way of mapping the appropriate Hamiltonian and master equation onto stochastic equations for *c*-number variables. In the present case, the only one of these representations which allows an exact mapping of our problem onto stochastic differential equations is the functional positive-*P* representation. This has previously been used to treat photoassociation [4,5], but numerical integration of the resulting equations is very time consuming and can present serious stability problems [7]. Hence we will use a truncated functional Wigner representation, which is much more stable and lends itself more readily to the modeling of different initial quantum states of the atomic condensate. A full Wigner representation of this problem would have derivatives of third order in the equation of motion for the pseudoprobability function, and, while it is possible to model these using stochastic difference equations [29], there are severe practical difficulties involved. However, as is commonly done with the Wigner representation, we can discard the third-order derivatives, which in this case leaves us with a Fokker-Planck equation with no diffusion matrix. This can be immediately mapped onto differential equations which have the appearance of coupled Gross-Pitaevskii-type equations. It must be stressed that there are, however, two important differences. First, averages must be taken over a large number of integrations of these equations, with initial conditions chosen so as to represent the Wigner function for the desired quantum states. Only if the Wigner function were to be a Dirac δ, which is completely nonphysical, would we recover the Gross-Pitaevskii equations. It is the probabilistic distribution of the initial state which allows the evolution of complex variables to represent (to a very good approximation) the evolution of noncommuting field operators. Second, being an approximation to the full Wigner representation, the truncated Wigner representation yields symmetrically ordered operator averages [30]. Formulas for physical quantities which are expressed as normally ordered operator averages must be corrected due to the operator reordering, as done in Eq. (13) below. With these reservations in mind, we can now model the interacting quantum fields via equations which are completely classical in appearance and hence lend themselves to a relatively simple numerical treatment.

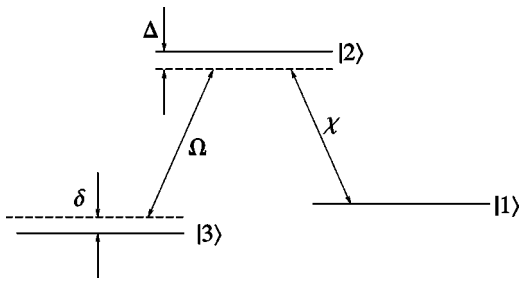

FIG. 1. Energy-level schematic of the coupled atomic and molecular fields. $|1\rangle$ represents the condensed atoms, $|2\rangle$ the excited molecules, and $|3\rangle$ the condensed ground-state molecules. The Raman laser coupling strengths are represented by χ and Ω, with Δ representing the detuning from the excited molecular band and δ representing the Raman detuning.

III. THE SYSTEM AND EQUATIONS OF MOTION

We consider that the initial atomic condensate is trapped such that one of the frequencies (ω_0) is much smaller than the other two, leading to a cigar shaped condensate which may be approximated as one dimensional. We consider here a two laser Raman photoassociation scheme [3–5] where the excited molecular field will be adiabatically eliminated. The three different atomic and molecular fields with the laser couplings and detunings are shown schematically in Fig. 1, with the process being described by the functional Hamiltonian (note that we use units such that $\hbar=1$)

$$\hat{H}=\int dx\,\hat{\psi}_a^\dagger(x)\left[-\frac{1}{2m}\frac{\partial^2}{\partial x^2}+V_a(x)\right]\hat{\psi}_a(x)+\int dx\,\hat{\psi}_{m*}^\dagger(x)$$
$$\times\left[-\frac{1}{4m}\frac{\partial^2}{\partial x^2}+V_{m*}(x)-\Delta\right]\hat{\psi}_{m*}(x)+\int dx\,\hat{\psi}_m^\dagger(x)$$
$$\times\left[-\frac{1}{4m}\frac{\partial^2}{\partial x^2}+V_m(x)+\delta\right]\hat{\psi}_m(x)+\frac{1}{2}\int dx[\,\hat{\psi}_a^{\dagger 2}U_{aa}\hat{\psi}_a^2$$

$$+\hat{\psi}_m^{\dagger 2}U_{mm}\hat{\psi}_m^2+2\hat{\psi}_a^\dagger\hat{\psi}_m^\dagger U_{am}\hat{\psi}_a\hat{\psi}_m]+\frac{i}{2}\int dx\chi(x)$$

$$\times[\hat{\psi}_a^{\dagger 2}(x)\hat{\psi}_{m*}(x)-\hat{\psi}_a^2(x)\hat{\psi}_{m*}^\dagger(x)]+i\int dx\Omega(x)$$

$$\times[\hat{\psi}_{m*}^\dagger(x)\hat{\psi}_m(x)-\hat{\psi}_{m*}(x)\hat{\psi}_m^\dagger(x)], \tag{1}$$

where m is the atomic mass, $\hat{\psi}_a(x)$ is the atomic field annihilation operator, $\hat{\psi}_{m*}(x)$ is the excited molecular-field annihilation operator, and $\hat{\psi}_m(x)$ is the ground-state molecular-field annihilation operator. The Rabi frequency of the transition between atoms and excited molecules is represented by $\chi(x)$ and $\Omega(x)$ is the Rabi frequency of the transition between excited and ground-state molecules. In principle, these could also be time dependent. The bare detunings Δ and δ are as shown in Fig. 1. The trapping potentials are represented by V_a (atoms), V_m (molecules), and V_{m*} (excited molecules). In the standard s-wave δ-function approximation, U_{aa} is the atom-atom interaction strength, U_{mm} represents that between molecules, and U_{am} represents atom-molecule scattering. Note that we are considering only one field for the excited molecules as the lasers should be detuned so that their population will remain as small as possible. For this reason, and also because the strengths are not at all known, we have ignored spontaneous breakup of the excited molecules and any collisional interactions involving them.

Following the usual route [7,31], we find a seemingly simple form for the master equation,

$$i\frac{d\rho}{dt}=[\hat{H},\rho], \tag{2}$$

as in our $T=0$ treatment there is no interaction with the environment. Although, given the problems with the size of the necessary Hilbert space, we can do nothing directly with this equation, it can be mapped onto a generalized functional Fokker-Planck equation for the Wigner distribution. This process gives the following equation, where $\psi_j(j=a,m,m^*)$ are now the complex variables of the Wigner representation:

$$\frac{\partial W}{\partial t}=\int dx\Bigg(-i\Bigg\{-\frac{\partial}{\partial\psi_a}\left[\frac{-1}{2m}\frac{\partial^2}{\partial x^2}+V_a(x)+U_{aa}(|\psi_a|^2-1)+U_{am}\left(|\psi_m|^2-\frac{1}{2}\right)\right]\psi_a-\frac{\partial}{\partial\psi_a^*}\left[\frac{1}{2m}\frac{\partial^2}{\partial x^2}-V_a(x)\right.$$

$$\left.-U_{aa}(|\psi_a|^2-1)-U_{am}\left(|\psi_m|^2-\frac{1}{2}\right)\right]\psi_a^*-\frac{\partial}{\partial\psi_{m*}}\left(\frac{-1}{4m}\frac{\partial^2}{\partial x^2}+V_{m*}(x)-\Delta\right)\psi_{m*}-\frac{\partial}{\partial\psi_{m*}^*}\left(\frac{1}{4m}\frac{\partial^2}{\partial x^2}-V_{m*}(x)+\Delta\right)$$

$$\times\psi_{m*}^*-\frac{\partial}{\partial\psi_m}\left[\frac{-1}{4m}\frac{\partial^2}{\partial x^2}+V_m(x)+U_{mm}(|\psi_m|^2-1)+U_{am}\left(|\psi_a|^2-\frac{1}{2}\right)+\delta\right]\psi_m-\frac{\partial}{\partial\psi_m^*}\left[\frac{1}{4m}\frac{\partial^2}{\partial x^2}-V_m(x)\right.$$

$$\left.-U_{mm}(|\psi_m|^2-1)-U_{am}\left(|\psi_a|^2-\frac{1}{2}\right)-\delta\right]\psi_m^*\Bigg\}-\chi(x)\left[\frac{\partial}{\partial\psi_a}\psi_a^*\psi_{m*}+\frac{\partial}{\partial\psi_a^*}\psi_a\psi_{m*}^*-\frac{1}{2}\left(\frac{\partial}{\partial\psi_{m*}}\psi_a^2+\frac{\partial}{\partial\psi_{m*}^*}\psi_a^{*2}\right)\right]$$

$$-\Omega(x)\left[\frac{\partial}{\partial\psi_{m*}}\psi_m+\frac{\partial}{\partial\psi_{m*}^*}\psi_m^*-\frac{\partial}{\partial\psi_m}\psi_{m*}-\frac{\partial}{\partial\psi_m^*}\psi_{m*}^*\right]-\frac{i}{4}\left[U_{aa}\left(\frac{\partial^3}{\partial\psi_a^2\partial\psi_a^*}\psi_a-\frac{\partial^3}{\partial\psi_a\partial\psi_a^{*2}}\psi_a^*\right)\right.$$

$$+U_{mm}\left(\frac{\partial^3}{\partial\psi_m^2\partial\psi_m^*}\psi_m-\frac{\partial^3}{\partial\psi_m\partial\psi_m^{*2}}\psi_m^*\right)+U_{am}\left(\frac{\partial^3}{\partial\psi_a\partial\psi_a^*\partial\psi_m}\psi_m+\frac{\partial^3}{\partial\psi_a\partial\psi_m\partial\psi_m^*}\psi_a-\frac{\partial^3}{\partial\psi_a^*\partial\psi_m\partial\psi_m^*}\right.$$

$$\left.\left.\times\psi_a^*-\frac{\partial^3}{\partial\psi_a\partial\psi_a^*\partial\psi_m^*}\psi_m^*\right)\right]+\frac{\chi(x)}{8}\left(\frac{\partial^3}{\partial\psi_a^2\partial\psi_{m*}^*}+\frac{\partial^3}{\partial\psi_a^{*2}\partial\psi_{m*}}\right)\Bigg)W(\psi_a,\psi_a^*,\psi_{m*},\psi_{m*}^*,\psi_m,\psi_m^*,t). \tag{3}$$

As stated above, although stochastic difference equations can be found which are equivalent to this generalized Fokker-Planck equation, they are difficult to use. Hence, by neglecting the third-order derivatives, we make a mapping onto a coupled set of differential equations. Although the neglect of these derivatives may be thought of as an uncontrolled approximation, it is an approximation that has previously given good results in many systems, especially when we only wish to calculate intensities. We note here that for a previous treatment of photoassociation using the positive-P representation [4], the truncated Wigner representation gives almost identical predictions for the atomic and molecular numbers.

Using the standard oscillator units, with time measured in units of ω_0^{-1} and space in units of $\sqrt{\hbar/m\omega_0}$, and considering the laser couplings as spatially constant across the trap, we find

$$i\frac{d\psi_a}{dt}=\left[-\frac{\partial^2}{\partial x^2}+V_a(x)+U_{aa}(|\psi_a|^2-1)+U_{am}\left(|\psi_m|^2-\frac{1}{2}\right)\right]\psi_a+i\chi\psi_a^*\psi_{m*},$$

$$i\frac{d\psi_{m*}}{dt}=\left(-\frac{1}{2}\frac{\partial^2}{\partial x^2}+V_{m*}(x)-\Delta\right)\psi_{m*}-\frac{i\chi}{2}\psi_a^2+i\Omega\psi_m,$$

$$i\frac{d\psi_m}{dt}=\left[-\frac{1}{2}\frac{\partial^2}{\partial x^2}+V_m(x)+U_{mm}(|\psi_m|^2-1)+U_{am}\left(|\psi_a|^2-\frac{1}{2}\right)+\delta\right]\psi_m-i\Omega\psi_{m*}. \quad (4)$$

It must be stressed here that, although these equations have the form of coupled equations of the Gross-Pitaevskii type, they are not equations for the order parameter, the mean fields, or for what are commonly called the macroscopic wave functions. They are equations for the complex variables of the Wigner representation of the three coupled condensates and these variables are in fact stochastic, with the initial conditions obeying a probability distribution. There are also differences in the self- and cross-interaction terms, which come purely from the Wigner distribution and will be seen below to cause a shift in the Raman detuning.

Although we could integrate the system of three equations, this would be rather time consuming. We will therefore take advantage of the fact that the Raman lasers should be detuned so as to create as few as possible of the excited molecules, as these have extremely short lifetimes and their spontaneous breakup would be a source of undesirable losses. We therefore adiabatically eliminate the equation for ψ_{m*} to leave two coupled equations for the complex atomic (ψ_a) and molecular (ψ_m) fields. By neglecting the kinetic energy in the equation for ψ_{m*} and assuming that these excited molecules are untrapped, we find

$$\psi_{m*}=\frac{-i}{\Delta}\left(\frac{1}{2}\chi\psi_a^2-\Omega\psi_m\right), \quad (5)$$

which can now be substituted into the equations for ψ_a and ψ_m. This process adds

$$\frac{\chi^2}{2\Delta}|\psi_a|^2\psi_a-\frac{\Omega\chi}{\Delta}\psi_a^*\psi_m \quad (6)$$

to the equation for ψ_a, and

$$\frac{\Omega\chi}{2\Delta}\psi_a^2-\frac{\Omega^2}{\Delta}\psi_m \quad (7)$$

to the equation for ψ_m. What we note is that, as well as the effective Raman coupling terms between atoms and molecules now depending on both fields plus the detuning from the excited level, a nonlinear light shift has been added to the atomic field and a linear light shift has been added to the molecular field. Setting $U'_{aa}=U_{aa}+\chi^2/2\Delta$, we see that the laser fields cause an effective change in the atom-atom scattering strength.

We can now write a pair of coupled equations which describe the system. Defining the frequency

$$\overline{\omega}=U_{aa}+\frac{U_{am}}{2}, \quad (8)$$

we use an atomic (molecular) frame rotating at $\overline{\omega}(2\overline{\omega})$ and introduce a fixed phase shift so that the Raman couplings are real. Finally, setting

$$\kappa=\frac{\Omega\chi}{\Delta},$$

$$\delta'=\delta+U_{mm}-2U_{aa}-\frac{U_{am}}{2}+\frac{\Omega^2}{\Delta}, \quad (9)$$

we find

$$i\frac{d\psi_a}{dt}=-\frac{\partial^2\psi_a}{\partial x^2}+V_a(x)\psi_a+(U'_{aa}|\psi_a|^2+U_{am}|\psi_m|^2)\psi_a+i\kappa\psi_a^*\psi_m$$

$$i\frac{d\psi_m}{dt}=-\frac{1}{2}\frac{\partial^2\psi_m}{\partial x^2}+V_m(x)\psi_m+(U_{mm}|\psi_m|^2+U_{am}|\psi_a|^2-\delta')\psi_m-\frac{i}{2}\kappa\psi_a^2. \quad (10)$$

The detuning from the Raman resonance is now represented by δ', which we will assume to be zero in our treatment. Note that we ignore interactions with any atoms of the thermal cloud which is usually found along with the condensed portion, as we are assuming that the condensate actually is at 0 K. In all our investigations we will use $U_{am}=-1.5U'_{aa}$, $U_{mm}=2U'_{aa}$, $\kappa=1$, $\delta'=0$, and a molecular trapping potential twice that of the harmonic atomic potential.

IV. EFFECT OF THE TRAPPING POTENTIAL

One of the things we wish to consider in this work is the effect that different trapping potentials may have on the process of photoassociation. Experimentally, there is some freedom in engineering the actual potential, as shown in a recent article by Thomas *et al.*, which describes the fabrication of a double-well trap for condensates [23]. During the adiabatic evolution from the original harmonic trap, a stage is passed where the bottom of the trap is much flatter. A trap of this form may well be interesting for photoassociation experiments, as the conversion rates effectively depend on the local densities through the products $\psi_a^*\psi_m$ and ψ_a^2. In Fig. 2 we compare the densities $|\psi_a(x)|^2$ for atomic condensates confined in differently shaped traps. The trap with a central potential of the form $V(x)\propto\sin^6 x$ gives a flatter density distribution than a harmonic trap, while a trap with $V(x)\propto\sin^2 x$

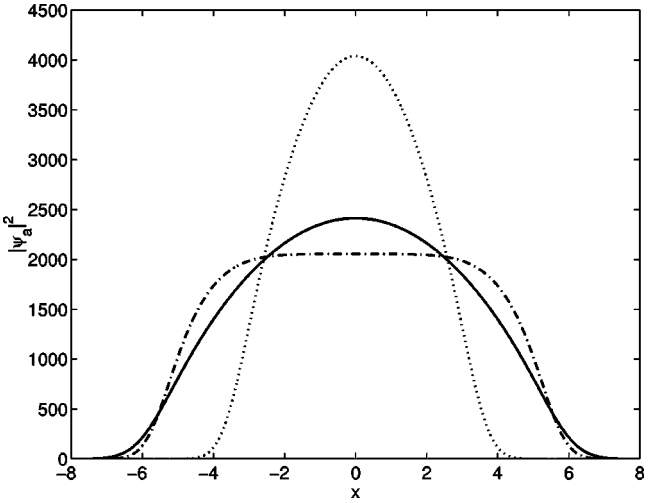

FIG. 2. Ground-state solutions of the Gross-Pitaevskii equation for a harmonic trap (solid line), a trap with $V_a(x) = 0.125x_{max}^2 \sin^6(\pi x/x_{max})$ (dash-dotted line), and $V_a(x) = 0.125x_{max}^2 \sin^2(\pi x/x_{max})$ (dotted line), with $x_{max} = 12$. The units of the spatial axis are $\sqrt{\hbar/m\omega_0}$.

gives a more peaked density distribution. If the different conversion rates at different spatial points were the only cause of dampening in the oscillations between the atoms and molecules which we will see below, we might think that a flatter trap could lead to more regular oscillations between the atomic and molecular condensates. This is because a flatter central density distribution is more like a homogeneous condensate. On the other hand, the more peaked distribution might then be expected to give less regularity in the oscillations, as there is more local-density variation across the center of the distribution. We will investigate these suppositions in what follows.

A. Harmonic trap

As a harmonic trapping potential is most commonly used in theoretical investigations of trapped condensates, we begin by considering this case. For purposes of comparison, we numerically integrate the GPE-type equations, which give semiclassical results with the quantum statistics playing no part in the time evolution. We emphasize here that the GPE solutions are not really physically relevant where they disagree with the quantum predictions, as it is impossible to turn off the quantum noise. What we find is that the spatial dependence of the trapped condensates plays an important role in the process, with the coupling rates at different densities being different. For the parameters used, this causes an interesting structure to emerge, with spatial sidebands forming in the distributions, as shown in a previous work [8]. Over the times shown here, the kinetic energy of the condensates has little effect, with an averaging of the results of integration of spatially separate single-mode equations at each spatial point giving virtually identical predictions, both spatially and for the total particle numbers. This is not the case for longer interaction times, where the atoms have time to move around due to both the trapping potential and the *s*-wave scattering processes.

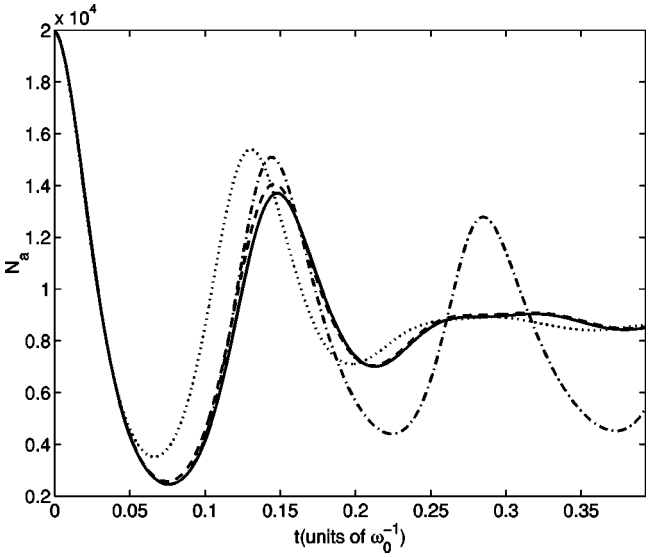

FIG. 3. Atomic population predictions in the harmonic trap, up to $t = \pi/8$. The dash-dotted line is from the GPE approach, the solid line is for an initial coherent state, the dashed line is the slightly sheared state, and the dotted line is the crescent state. All quantities plotted in this and subsequent graphs are dimensionless.

In Figs. 3 and 4 we show the mean particle numbers, defined as

$$N_j = \Delta x \sum_k \left(\overline{|\psi_j(x_k)|^2} - 1/2\Delta x \right), \tag{11}$$

where $j = a, m$, and k labels the points on the numerical grid. What we see is that when we use an initial coherent state in the Wigner equations, we do not find the dramatic differences from the GPE predictions for the first atomic revival as reported previously [4,5]. The reason is simply that we are working with different parameters, with the ratio between κ and the strength of the nonlinear interactions being important in this regard. This was previously demonstrated to be the

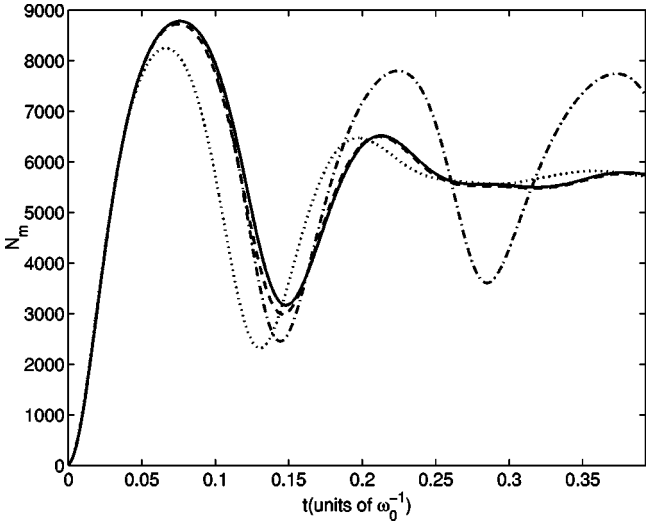

FIG. 4. Molecular population predictions in the harmonic trap, with lines as in Fig. 3.

case in traveling wave second-harmonic generation, with which, although it is not as rich a system as coupled condensates, a useful analogy can be made [20]. What we do see is that the oscillations predicted by Heinzen *et al.* [3] do not persist after the first atomic revival, once the quantum noise is taken into account. This feature is not due to interactions with thermal atoms, as in Góral *et al.* [32], as there are no thermal atoms present in our zero temperature treatment. Nor is it due merely to an averaging over different conversion rates at different positions within the condensates, as this averaging effect is also present in the GPE treatment. It is due to the quantum nature of the matter fields, cannot be represented by classical treatments, and is intrinsic to the process of photoassociation. Whether and to what extent the oscillations may be more persistent for different parameter regimes, for example larger condensates or different initial states, is an open question.

An initial atomic state with the same degree of amplitude squeezing and shearing as calculated in Ref. [15] also does not lead to vastly different dynamics from the initial coherent state, the difference between the two being almost negligible. However, a dramatic difference in the early dynamics occurs when we consider the initial *crescent* state (see Sec. 1 of the Appendix below), which is greatly sheared in phase space with a large degree of number squeezing (the single-mode Fano factor for this distribution is ≈ 0.2), but being well above the minimum uncertainty product in the quadratures [single-mode $V(X) \approx 0.6, V(Y) \approx 15$]. The initial conversion to molecules for this state is not as complete and the first revival in the atomic population is earlier and more pronounced than that for the other initial states. Interestingly enough, the longer time behavior is almost independent of the initial state, with the populations reaching a quasistationary state. Whether a later revival of the oscillations is present or not is difficult to predict using our methods, as the computational time required becomes prohibitive. However, we consider it unlikely as the system of interacting atomic and molecular condensates is probably too complicated to find the collapses and revivals predicted in, for example, the Jaynes-Cummings model [33].

As the initial conversion rates for all the states considered here were almost identical, it seems that the differences seen are not due to the spatial intensity correlation, defined using the field operators as

$$g^{(2)}(x,x) = \frac{\langle \hat{\psi}_a^\dagger(x)\hat{\psi}_a^\dagger(x)\hat{\psi}_a(x)\hat{\psi}_a(x)\rangle}{\langle \hat{\psi}_a^\dagger(x)\hat{\psi}_a(x)\rangle^2}. \tag{12}$$

This correlation factor is predicted to be important in the initial conversion rate for both traveling wave second harmonic generation and photoassociation of homogeneous condensates [18,34]. In the variables of the Wigner representation, which represent symmetrically ordered operator averages, the definition is

$$g^{(2)}(x,x) = \frac{\overline{|\psi_a(x)|^4} - 2\overline{|\psi_a|^2} + 1/2\Delta x}{(\overline{|\psi_a(x)|^2} - 1/2\Delta x)^2}. \tag{13}$$

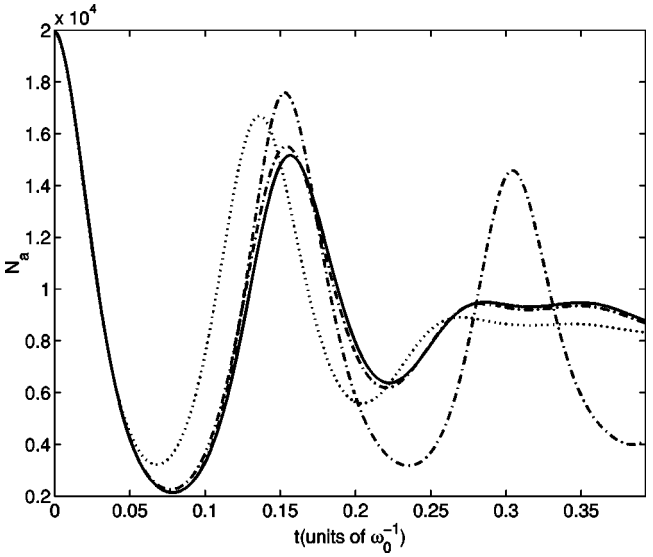

FIG. 5. Atomic population predictions up to $t = \pi/8$ in the flatter trap, with $V(x) \propto \sin^6 x$. The lines are as in Fig. 3.

The values found vary between 1 and 1.04 at the center for the initial states considered here in the harmonic trap, with the initial conversion rate almost unchanged. The differences come in the first minimum of the atomic population and the subsequent revival and are more readily explained by the degree of phase uncertainty in the initial state. It can be seen by examination of Eq. (10) that whether association or disassociation is predominant will partially depend on the phase of the products $\psi_a^* \psi_m$ and ψ_a^2. As the crescent state has a larger phase uncertainty than the others considered, the photodisassociation process begins to dominate and the mean number of atoms begins to revive at an earlier time than for the other states.

B. Other trapping potentials

When we investigate the effect of the three different traps considered, we do find differences in the oscillations predicted, but we do not find that these are noticeably more persistent for any particular trap shape. In Fig. 5 we show the results for the trap with $V_a(x) = 0.125 x_{max}^2 \sin^6(\pi x/x_{max})$, with $x_{max} = 12$. These are in fact not very different at all from those for the harmonic trap and we again do not see more than one large revival of the atomic number. Figure 6, for $V_a(x) = 0.125 x_{max}^2 \sin^2(\pi x/x_{max})$, also shows similar dynamics, but the initial conversion rate is a little higher, being dependent on the density. Note that in all cases we assume that the ground-state molecules are trapped by a potential of the same form and with twice the intensity of the atomic trap. This is consistent with harmonic traps for atoms, where $V(x) = \frac{1}{2} m \omega_0^2 x^2$, since the mass of a molecule is twice that of an atom. We have assumed that this relationship also holds for other trapping potentials considered here.

In Fig. 7, we compare the atomic evolution for the initial crescent state in the three different traps, showing clearly that, while there are differences in the time evolution, the end results after a short interaction time are virtually the same.

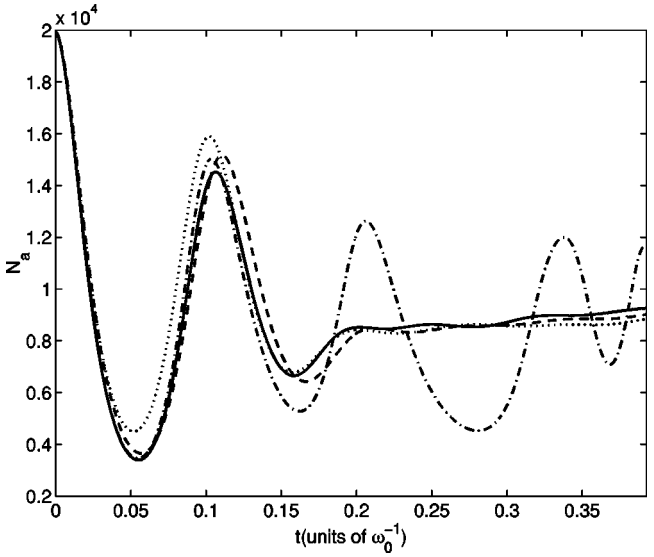

FIG. 6. Atomic population predictions up to $t=\pi/8$ in the narrow trap, with $V(x)\propto \sin^2 x$. The lines are as in Fig. 3.

The flatter traps show a slightly more complete conversion to molecules after the first revival of the atomic population, but the difference is not striking. Unlike the GPE predictions, we always find a quasistationary state where the conversion has almost stopped. It is not just the density integrated across the condensate which is almost unchanging, but the atomic and molecular numbers are also almost not changing at each point, as can be seen in Fig. 8. Although the result shown is for an initial coherent state in the harmonic trap, the other cases considered above do not give qualitatively different results. This effect, which we may think of as a saturation of the conversion rate, is not due solely to different conversion rates at each point or it would show up in the GPE predictions. It is due to the quantum nature of the condensate, and, while it does not require a fully quantum description (which the truncated Wigner does not provide for this system), quantum noise must be taken into account.

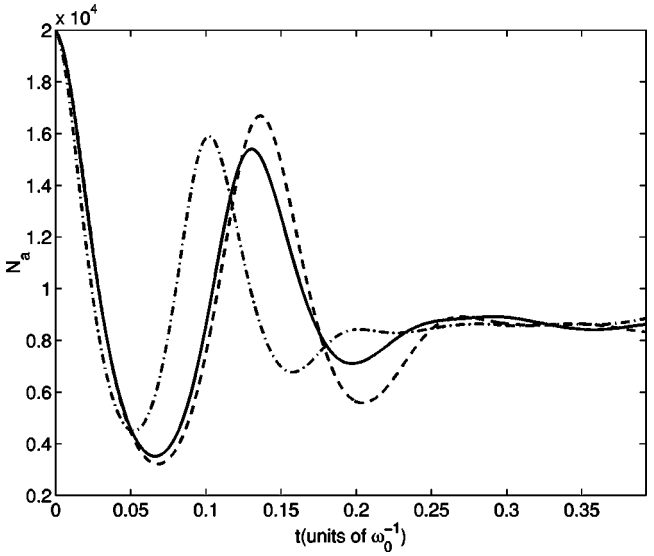

FIG. 7. Atomic population predictions up to $t=\pi/8$ for the initial crescent state, in the three different traps. The solid line is for the harmonic trap, the dash-dotted line is for $V(x)\propto \sin^2 x$, and the dashed line is for $V(x)\propto \sin^6 x$.

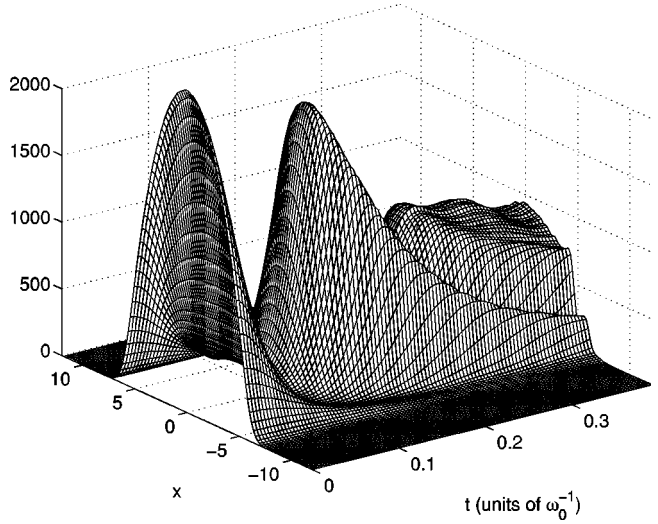

FIG. 8. Mean atomic field density up to $t=\pi/8$ for an initial coherent state in the harmonic trap. The units of the spatial axis are $\sqrt{\hbar/m\omega_0}$.

What we have not investigated in this paper are the effects of different initial atom numbers, Raman detunings, different *s*-wave scattering strengths, and perhaps even a spatially dependent Raman laser coupling. As the process is highly nonlinear, it is possible that the superchemistry-type oscillations predicted by Heinzen *et al.* [3] would be more persistent for different parameters, but we suspect that they may be difficult to reproduce experimentally. In any case, we are confident that for more than short interaction times, simulations which take the quantum noise into account will be necessary to accurately reproduce or predict the results of any superchemistry-type photoassociation experiment. Without doing this analysis, we can say little about the accuracy of the GPE approach for each situation.

V. THE ZERO-DIMENSIONAL APPROACH

This approach has been used, in a classical mean-field approximation, to represent Raman photoassociation of atomic condensates [35]. The claim has been made that to reproduce the results for a condensate with spatial dependence, all one needs to do is to take the average of integrations for different points from the spatially dependent condensate. If the condensate did in fact obey the mean-field equations this approach would actually give reasonable results for short times. For processes which take place over longer times, the kinetic energy has an effect and atoms and molecules can move around, changing the behavior. However, after a short time, the mean-field approach can give completely wrong predictions for the populations, even when we begin with coherent states. This has been previously seen in traveling wave second-harmonic generation [36,20], but is possibly not as important in that system due to the small nonlinearities and short interaction times of available $\chi^{(2)}$

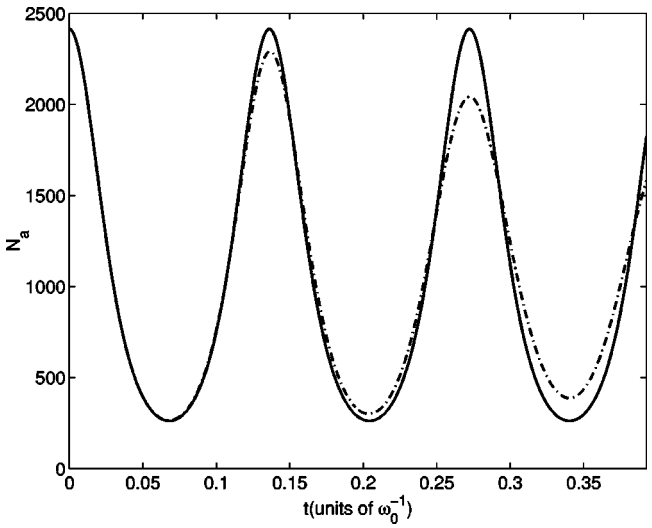

FIG. 9. Zero-dimensional predictions for the atomic population. The solid line represents the classical mean-field prediction, and the dash-dotted line is the stochastic prediction for an initial coherent state, averaged over 4.35×10^5 trajectories. In this case the other initial states do not show a noticeable difference from the coherent state.

materials. With photoassociation, however, we do not have the same limits on interaction time. The process will continue as long as the Raman lasers are switched on and the condensate remains stable, which should be sufficient to produce a large number of the superchemistry-type oscillations if the mean-field picture were correct.

We can investigate the zero-dimensional system with the coupled equations

$$\frac{d\alpha}{dt} = -i(U_{aa}|\alpha|^2 + U_{am}|\beta|^2)\alpha + \kappa\alpha^*\beta,$$

$$\frac{d\beta}{dt} = -i(U_{mm}|\beta|^2 + U_{am}|\alpha|^2 - \delta')\beta - \frac{\kappa}{2}\alpha^2, \qquad (14)$$

where α and β now represent atomic and molecular amplitudes, respectively. The other parameters are all as in Eq. (10). Note that the lack of potential and kinetic energy in this approach means that, apart from the detuning δ', these equations are mathematically equivalent to those used in Ref. [20]. One important difference from the optical case, however, is that the U_{ij} self- and cross-interaction terms are very much larger than those likely to be found in any optical system.

We show the results for the atomic dynamics in Fig. 9, comparing the predictions of the truncated Wigner with an initial coherent state to those of the classical approach, both for an initial atom number equal to $|\psi_a|^2$ at the center of the densities used for the harmonic trap. Note here that this is not the same as the atomic number at the center of the one-dimensional grid, which is $\Delta x|\psi_a|^2$, but is the number which enters into the one-dimensional equations. The results for the other initial quantum states considered above are virtually indistinguishable from the coherent state. We find that the classical approach, which predicts regular periodic behavior in this case, is reasonably accurate up to the second revival of atomic population, but then begins to differ from the quantum prediction. The quantum result shows a damping of the oscillations, due solely to the quantum noise. This serves to show that any averaging process using mean-field solutions would eventually become an averaging over erroneous values and could not be expected to lead to correct predictions. We note also that it is very easy to find parameter regimes where the classical and quantum predictions are markedly different, even for early times. In this regard, the ratio between κ and the *s*-wave interactions plays an important role, with the classical predictions becoming less accurate as κ/U_{aa} is increased.

VI. CONCLUSION

We have used a truncated Wigner representation to examine the dynamics of continuous-wave Raman BEC photoassociation, examining the effects of different initial quantum states and different trapping potentials. We have also examined the accuracy of the zero-dimensional, quantum-optics-type approach. What we have shown is that both the quantum state of the initial atomic condensate and the actual form of the confining potentials can play important roles in the dynamics of the mean fields. In none of the cases considered was the GPE approach accurate over more than short times. We found that the form of the trapping potential affects the rates of conversion, with a tighter trap and hence higher peak densities giving greater initial conversion rates, as expected. The superchemistry-type oscillations previously predicted in a GPE approach are not persistent for any of the combinations of traps and initial conditions considered here. This is true even at zero temperature, in which case any interaction with thermal atoms can play absolutely no part in the time evolution. All the quantum states considered exhibit different dynamics from the GPE predictions, especially as the interaction time increases. The phase sheared *crescent* state, possibly the most likely for BEC, gives the most marked differences. Over the time scales we considered, the quantum statistics are much more important than the spatial dependence of the condensate. These results suggest that, if we wish to simulate or predict the results of Raman photoassociation experiments, an analysis which takes into account the quantum nature of the interacting condensates will be important. It also suggests that if superchemistry-type oscillations are to be observed, a very careful choice of the experimental parameters will need to be made.

ACKNOWLEDGMENTS

This research was supported by the New Zealand Foundation for Research, Science and Technology (Grant No. UFRJ0001). The author thanks Ashton Bradley and Karen Kheruntsyan for valuable comments.

APPENDIX

1. Integration of the equations

For the purposes of comparison, in all simulations we used as our starting point a ground-state solution of the GPE

for a one-dimensional trapped atomic condensate with 2×10^4 atoms and a value of the nonlinear interaction, $U'_{aa}=4\times10^{-3}$. This solution for the initial condition is obtained via numerical propagation of the GPE in imaginary time [37], beginning with the Thomas-Fermi solution for these parameters and the appropriate trapping potential. The integration always begins with all particles in the atomic condensate and no molecules. The equations are averaged over 10^4 trajectories, using a standard split-operator method, with momentum propagation in Fourier space and a three-step predictor-corrector method in position space. The accuracy and stability of the integration is checked by keeping track of the conserved quantity, N_a+2N_m, and by varying the time step. Over the times shown, results with a halved time step were virtually indistinguishable and number was conserved to within less than 0.05%.

To model the intial quantum states of the condensates, each of the 512 points in the spatial grid is given an initial value on each trajectory, chosen from the Wigner distribution for the appropriate state. A coherent state is modeled by taking the (real) ground-state GPE solution for the nth spatial point and adding real and imaginary numbers drawn from a normal Gaussian distribution, giving $\psi_a(x_n)=\psi_a^{GP}(x_n)+0.5[\eta_1(x_n)+i\eta_2(x_n)]/\sqrt{\Delta x}$, where Δx is the spacing of the numerical grid. It is easily verified that the trajectory average will be $|\psi_{GP}(x_n)|^2+1/2\Delta x$ at each point, with $1/2\Delta x$ needing to be subtracted at each point once the trajectory averaging has taken place. A minimum uncertainty squeezed state is modeled by adding $0.5[\eta_1(x_n)e^{-r}+i\eta_2(x_n)e^{r}]/\sqrt{\Delta x}$ at each point, where r is the squeezing parameter. A sheared state, typical of Kerr nonlinearities, as in Dunningham *et al.* [15], is simulated by transforming the added squeezed state noise by a factor $\exp[iq\eta_3(x_n)]$, where q is the shearing factor. The real noise terms have the correlations

$$\overline{\eta_j(x_n)}=0,\quad \overline{\eta_i(x_m)\,\eta_j(x_n)}=\delta_{mn}\delta_{ij}\,. \tag{A1}$$

Numerical checks of single-mode distributions produced using these methods show that they give the expected values for average numbers and quadrature variances. In our simulations for squeezed states, we use values of $r=\pm\log 0.5$, while for the sheared state we used $q=0.005$, which give results similar to the Wigner function shown in Dunningham *et al.* [15]. We also investigate a more extreme shearing of the distribution, with $r=-\log 0.2$ and $q=0.05$, as we are treating a larger condensate than those considered in Refs. [15,16]. This will hence possess a larger effective Kerr nonlinearity and be expected to have a more sheared Wigner distribution. We call this choice of initial condition a *crescent* state, due to the shape of the contours of the resulting Wigner distribution. The molecular field always begins as a coherent vacuum, with $\psi_m(x_n)=0.5[\eta_4(x_n)+i\eta_5(x_n)]/\sqrt{\Delta x}$ on each trajectory, with the random variables defined as in Eq. (A1).

2. Interpretation of the Wigner distribution for atomic fields

The addition of noise terms in the initial condition of the Wigner equations, which calculate symmetrically ordered operator products, and gives as an average the normally ordered expectation value plus half an atom (or molecule) in each spatial mode, does not have a simple physical interpretation as with optical fields. With the Wigner representation in optics, a natural interpretation is that there is *one-half of a vacuum photon* in each mode. This is indeed the interpretation given in the classical theory of stochastic electrodynamics [38], which is equivalent to the truncated Wigner representation and explains nonlinear optical processes as classical evolution under the effects of vacuum noise. It has been used to explain many effects, such as quadrature squeezing, which do not require a negativity of the Wigner function. The P representations, on the other hand, calculate normally ordered operator products and any nonclassical effect is explained as being due to interaction with a nonlinear medium. In the case of bosonic matter fields, the extra half *vacuum atom* should be thought of only as a mathematical device which allows classical variables to represent symmetrically ordered operator moments. The difficulty of considering that these half vacuum atoms have any physical existence is made clear when we try to think of an atomic analog of the Casimir effect, which, in the electromagnetic case, can be explained very well by stochastic electrodynamics as being due to the absence of some half vacuum photons between the two plates. In the atomic case, we would have to consider that the analogous force existed due to every type of bosonic atom (and molecule?) that was not present between the equivalent of the two plates, which seems absurd. As always in quantum mechanics, what is real is that which can be observed in some way, which in the present case are normally ordered products of the matter fields. Obviously, these normally ordered products need not have integer values, but will always have half an atom less in each mode than the average number predicted by the Wigner representation. Given this caveat as to interpretation, we can use the Wigner representation equations to calculate the time evolution of the interacting atomic and molecular condensates.

[1] P.D. Drummond, K.V. Kheruntsyan, and H. He, Phys. Rev. Lett. **81**, 3055 (1998).
[2] J. Javanainen and M. Mackie, Phys. Rev. A **59**, R3186 (1999).
[3] D.J. Heinzen, R. Wynar, P.D. Drummond, and K.V. Kheruntsyan, Phys. Rev. Lett. **84**, 5029 (2000).
[4] J.J. Hope and M.K. Olsen, Phys. Rev. Lett. **86**, 3220 (2001).
[5] J.J. Hope, Phys. Rev. A **64**, 053608 (2001).
[6] P.D. Drummond and C.W. Gardiner, J. Phys. A **13**, 2353 (1980).
[7] M.J. Steel, M.K. Olsen, L.I. Plimak, P.D. Drummond, S.M. Tan, M.J. Collett, D.F. Walls, and R. Graham, Phys. Rev. A **58**, 4824 (1998).
[8] M.K. Olsen and L.I. Plimak, Phys. Rev. A **68**, 031603 (2003).
[9] E.L. Bolda, S.M. Tan, and D.F. Walls, Phys. Rev. A **57**, 4686

(1998).
[10] S. Mancini, M. Fortunato, P. Tombesi, and G.M. D'Ariano, J. Opt. Soc. Am. A **17**, 2529 (2000).
[11] M.R. Andrews, C.G. Townsend, H.J. Meisner, D.S. Durfee, D.M. Kurn, and W. Ketterle, Science **275**, 637 (1997).
[12] W. Ketterle and H.J. Miesner, Phys. Rev. A **56**, 3291 (1997).
[13] J.M. Vogels, J.K. Chin, and W. Ketterle, Phys. Rev. Lett. **90**, 030403 (2003).
[14] M. Lewenstein and L. You, Phys. Rev. Lett. **77**, 3489 (1996).
[15] J.A. Dunningham, M.J. Collett, and D.F. Walls, Phys. Lett. A **245**, 49 (1998).
[16] J. Rogel-Salazar, S. Choi, G.H.C. New, and K. Burnett, Phys. Lett. A **299**, 476 (2002).
[17] V. Chernyak, S. Choi, and S. Mukamel, Phys. Rev. A **67**, 053604 (2003).
[18] Y.R. Shen, Phys. Rev. **155**, 921 (1967).
[19] M.K. Olsen, L.I. Plimak, and A.Z. Khoury, Opt. Commun. **201**, 373 (2002).
[20] V.I. Kruglov and M.K. Olsen, Phys. Rev. A **64**, 053802 (2001).
[21] A. Sinatra, C. Lobo, and Y. Castin, Phys. Rev. Lett. **87**, 210404 (2001).
[22] A. Sinatra, C. Lobo, and Y. Castin, J. Phys. B **35**, 3599 (2002).
[23] N.R. Thomas, A.C. Wilson, and C.J. Foot, Phys. Rev. A **65**, 063406 (2002).
[24] L.P. Pitaevskii, Zh. Éksp. Teor. Fiz. **40**, 646 (1961) [Sov. Phys. JETP **13**, 451 (1961)].
[25] E.P. Gross, Nuovo Cimento **20**, 454 (1961).
[26] W. Krauth, Phys. Rev. Lett. **77**, 3695 (1996).
[27] I. Carusotto, Y. Castin, and J. Dalibard, Phys. Rev. A **63**, 023606 (2001).
[28] C.W. Gardiner, J.R. Anglin, and T.I.A. Fudge, J. Phys. B **35**, 1555 (2002).
[29] L.I. Plimak, M.K. Olsen, M. Fleischhauer, and M.J. Collett, Europhys. Lett. **56**, 372 (2001).
[30] L.I. Plimak, M. Fleischhauer, M.K. Olsen, and M.J. Collett, e-print cond-mat/0102483.
[31] C.W. Gardiner, *Quantum Noise* (Springer-Verlag, Berlin 1991).
[32] K. Góral, M. Gajda, and K. Rzążewski, Phys. Rev. Lett. **86**, 1397 (2001).
[33] J.H. Eberly, N.B. Narozhny, and J.J. Sanchez-Mondragon, Phys. Rev. Lett. **44**, 1323 (1980).
[34] K.V. Kheruntsyan, D.M. Gangardt, P.D. Drummond, and G.V. Shlyapnikov, Phys. Rev. Lett. **91**, 040403 (2003).
[35] M. Koštrun, M. Mackie, R. Côté, and J. Javanainen, Phys. Rev. A **62**, 063616 (2000).
[36] M.K. Olsen, R.J. Horowicz, L.I. Plimak, N. Treps, and C. Fabre, Phys. Rev. A **61**, 021803 (2000).
[37] H. Wallis, A. Röhrl, M. Naraschewski, and A. Schenzle, Phys. Rev. A **55**, 2109 (1997).
[38] T.W. Marshall, Proc. R. Soc. London, Ser. A **276**, 475 (1963).